ACS APPLIED MATERIALS & INTERFACES

Article

Spatiotemporally Resolved Tracking of Bacterial Responses to ROS-Mediated Damage at the Single-Cell Level with Quantitative Functional Microscopy

Alvaro Barroso, Malte Christian Grüner, Taylor Forbes, Cornelia Denz, and Cristian Alejandro Strassert

ACS Appl. Mater. Interfaces, **Just Accepted Manuscript** • DOI: 10.1021/acsami.6b02605 • Publication Date (Web): 26 May 2016

Just Accepted

ACS Publications

ACS Applied Materials & Interfaces is published by the American Chemical Society.
1155 Sixteenth Street N.W., Washington, DC 20036

Spatiotemporally Resolved Tracking of Bacterial Responses to ROS-Mediated Damage at the Single-Cell Level with Quantitative Functional Microscopy

Álvaro Barroso,[a,†] *Malte Grüner,*[b,†] *Taylor Forbes,*[a] *Cornelia Denz,*[*,a] *and Cristian A. Strassert*[*,b]

[a]Institut für Angewandte Physik and Center for Nonlinear Science (CeNoS)
Westfälische Wilhelms-Universität Münster, Corrensstraße 2, D-48149 Münster (Germany)
[b]Physikalisches Institut and Center for Nanotechnology (CeNTech)
Westfälische Wilhelms-Universität Münster, Heisenbergstraße 11, D-48149 Münster (Germany)

[†]Co-first authors that equally contributed to this work
*Corresponding authors. E-mail: denz@uni-muenster.de; ca.s@wwu.de

Keywords:
Photoactive particles, quantitative functional microscopy, reactive oxygen species, bacteria, optical tweezers, phototherapy

Abstract

Herein we report on the implementation of photofunctional microparticles in combination with optical tweezers for the investigation of bacterial responses to oxidative stress by means of quantitative functional microscopy. A combination of a strongly hydrophobic axially substituted Si(IV) phthalocyanine adsorbed onto silica microparticles was developed, and the structural and photophysical characterization was carried out. The microparticles are able to produce reactive oxygen species under the fluorescence microscope upon irradiation with red light, and the behaviour of individual bacteria can be consequently investigated *in situ* and *in real time* at single cell level. For this purpose, a methodology was introduced to monitor phototriggered changes with spatiotemporal resolution. The defined distance between the photoactive particles and individual bacteria can be fixed under the microscope before the photosensitization process is started, and the photoinduced damage can be monitored by tracing the time-dependent fluorescence turn-on of a suitable marker. The results showed a distance-dependent photoinduced death time, defined as the onset of the incorporation of propidium iodide. Our methodology constitutes a new tool for the *in vitro* design and evaluation of photosensitizers for the treatment of cancer and infectious diseases with the aid of functional optical microscopy, as it enables a quantitative response evaluation of living systems towards oxidative stress. More generally, it provides a way to understand the response of an ensemble of living entities to reactive oxygen species by analyzing the behavior of a set of individual organisms.

Introduction

Emerging resistances against antibiotics are considered to be one of the major challenges of the 21st century.[1,2] Photodynamic therapy (PDT) constitutes a treatment for numerous diseases including cancer, mycosis and bacterial infections.[3–5] A photosensitizer (PS) is administered systemically, locally or topically to the site of the biological target.[6] Upon application of harmless visible light, cytotoxic singlet oxygen ($^1O_2$) is generated by energy transfer from the excited PSs' chromophore to triplet oxygen ($^3O_2$).[7,8] $^1O_2$ chemically reacts with organic substrates within its diffusion range of 268 nm, affecting biological membranes, and ultimately inducing cell death.[9] A fundamental understanding of the processes that take place during the photodynamic inactivation (PDI) is crucial for the rational design of PSs. It includes the kinetic and dynamic factors related to extra- and intracellular $^1O_2$ or derived reactive oxygen species (ROS).[10]

With the idea of developing platforms for the immobilization and local delivery of these photodynamic dyes, it has been suggested to combine PSs with a variety of vehicles (as e.g. liposomes, micelles, and PS conjugates with nano- and microparticles). For example, microparticles with aqueous compatibility were functionalized with PSs such as porphyrins and rose bengal and have found application in the bacterial decontamination of water, whereas micro-sized particles were used for three dimensional oxygen sensing in bacterial biofilms, and squaraine functionalized microparticles were applied for near-infrared imaging *in vivo*, only to mention a few.[11–14] Additionally, we have shown that photoactive nanomaterials based on zeolite L crystals can be suitably designed by axial binding of Si(IV) phthalocyanines to target, to label and to photoinactivate antibiotic-resistant Gram-negative pathogens such as *E. coli* and *N. gonorrhoeae.*[15,16] Moreover, we demonstrated the selective photodynamic inactivation of Gram-positive bacteria in the presence of Gram-negative bacteria by a photoactive nanomaterial based on a synthetic nanoclay capable of producing $^1O_2$.[17,18]

We have recently shown that photofunctional surfaces bearing PSs of diverse classes can be controlled regarding aggregation of the active chromophores.[19,20] They are also useful to design and to realize photoactive substrates for quantitative functional microscopy, facilitating the generation of ROS and monitoring responses of individual eukaryotic cells with spatiotemporal resolution directly under the fluorescence microscope.[21] Interestingly, it was observed that the evolution of phenotypical changes and cellular responses vary from one cell to another, also depending on the localization of the photoinduced damage (intracellular *vs.* extracellular ROS production). The quantitative evaluation of caspase activity at

single cell level provided a differentiated analysis of biological readouts from individual living entities, as opposed to the observation of the whole ensemble providing only population-averaged information. Established methods in microbiology for testing the photoinduced ROS-mediated cytotoxicity rely on techniques which measure the number of bacterial colonies originated from surviving cells by plating and counting colony forming units, or by flow cytometry with fluorescence detection. These methods, despite being very sensitive, provide information only about the overall toxicity produced to the whole bacterial ensemble, without giving information about individual entities and their particular interaction with ROS. However, due to the limited diffusion range of $^1O_2$, it is crucial to control its production at a defined distance from the biological target to understand the participation of derived long-lived ROS arising from the reaction of $^1O_2$ with organic molecules. Thus, in order to elucidate the underlying mechanisms, it is necessary to design defined scenarios with a full control over physical parameters, such as the distance between the bacteria and the spot of $^1O_2$ photoproduction. To understand these pheomena at the single cell level, novel methods are required that are capable of regulating the ROS production, monitoring the subsequent time-dependent damage inflicted to the bacteria cells as a function of the distance from the PS. Ideally, the *in situ* imaging and manipulation techniques should be minimally invasive and provide adequate readouts in real time with spatiotemporal resolution at single cell level.

Fluorescence microscopy provides a reliable toolbox for rapidly imaging the viability of living cells as a function of membrane integrity. By using organic dye probes which penetrate only the membrane of dead cells, *e.g.* propidium iodide (PI), trypan blue-exclusion or neutral red uptake, it is possible to obtain quantitative information about the viability. Among the manipulation methods, optical trapping techniques are of particular importance because of their versatility to trap and to move in a contactless and aseptic fashion diverse entities with a higher refractive index than the surrounding environment, as it is the case for particles, cells and bacteria. In particular, optical tweezers, which are able to confine transparent microscopic particles near the focus spot of a tightly focused laser beam by means of light gradient forces,[22] have been widely used for more than two decades for manipulating and controlling biological objects.[23] For example, they have been used to position bacteria at surfaces in a predetermined area,[24,25] and to investigate the adhesion of bacteria to inorganic surfaces, *e.g.* glass and functionalized coated microspheres.[26,27] Further on, holographic optical tweezers (HOT), which allow dynamic manipulation of several particles by tailoring the trapping beam into several single or even more complex optical traps,[28] have been demonstrated to extend the

versatility of conventional optical tweezers for studying the interactions of functionalized micro-sized materials with several biological targets. We have recently shown that HOT enable full 3D rotation and translation of multiple bacteria, optically-induced structuring of bacteria arrays and optical assembly of bio-hybrid micro-robots made of self-propelled bacteria and functionalized zeolite L crystals.[25,29,30]

In this work, we present a novel method that enables the quantitative spatiotemporally resolved photoproduction and analysis at the single bacterial level of the damage inflicted by ROS, combining HOT and microspheres functionalized with a tailored PS. A tetra-*tert*-butyl-substituted Si^{IV} phthalocyanine dihydroxide was functionalized with two axial trimethylsilane moieties in order to produce the highly hydrophobic PS **3**, which was then adsorbed onto the surface of 3 µm silica spheres (**MP**) to form **3@MP** microparticles. The photophysical characteristics were quantified for **3** (in CH_2Cl_2) as well as for **3@MP** (in water). We evaluated two different approaches based on HOT for the arrangement of defined spatial arrangements which allow investigating the bacterial response to ROS using **3@MP** in combination with *S. aureus* 6850. PI only intercalates in the DNA of the dead microorganisms, causing a fluorescence onset which was monitored to follow the inactivation of the microorganisms. We investigated the irradiation time that is required for damaging the bacteria at different distances with respect to the microspheres that generate $^1O_2$. The method presented herein therefore allows the spatiotemporally resolved investigation of the photoperturbation at single cell level. Thus, the behavior of the whole ensemble can be recovered by averaging the response of individual microorganisms. Moreover, it allows monitoring the diffusion capabilities of $^1O_2$ or derived ROS using bacteria as examples for biological targets, constituting a new step in the development of functional surfaces for quantitative functional microscopy.

Experimental Section

Materials. Silicon (IV)2,9,16,23-tetra-*tert*-butyl-29*H*,31*H*-phthalocyanine dihydroxide (**1**) was purchased from Sigma-Aldrich as well as the methoxytrimethylsilane (**2**). The solvents for the synthesis were purchased from Merck (analytical grade) and used without further purification. Deuterated solvents were used without further purification and purchased from Merck. For the spectroscopic characterization, spectroscopy-grade solvents were used from Merck and used as delivered. The particles were supplied by Kisker Biotech GmbH & Co. KG and used as supplied. According to the supplier, they were originally produced by Micromod Partikeltechnologie GmbH, with a pore size of about 100 ångström, and a BET surface of 350 m²/g. It is therefore unlikely that bacteria can diffuse into the pores.

Synthesis of 3. The synthesis was described previously by Stephen R. Cain *et al.* (*J. Phys. Chem.* **1991**, *95*, 9584-9589), but no characterization of the product was reported. We therefore optimized our own reaction conditions and characterized the obtained PS. 100 mg (0.125 mmol) of **1** were dissolved in 30 mL of pyridine and refluxed for 15 min (Scheme 1). Addition of 3 mL (21.76 mmol) of **2** and boiling for 14 h yielded the raw product. The pyridine was removed by vacuum evaporation at 50°C and the residue dissolved in EtOH and crystallized by addition of H_2O. Further purification by preparative thin-layer chromatography (ethylacetate: *n*-hexane = 1:4; R_f = 0.66) yielded 41 mg (0.044 mmol, 35%) of the desired product.

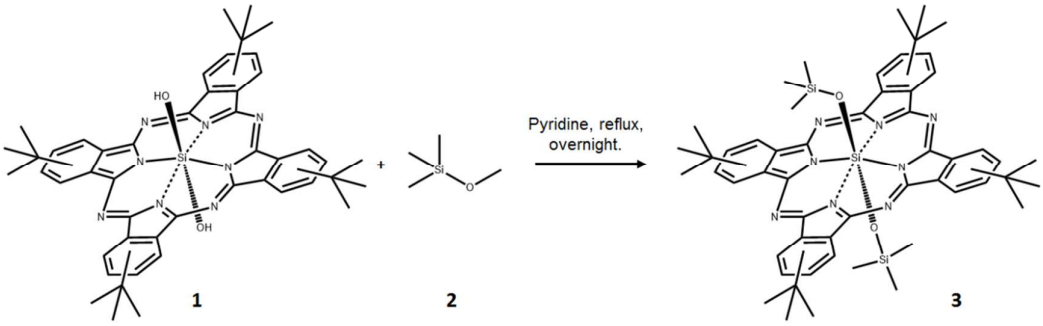

Scheme 1. Reaction pathway towards **3**.

UV-Vis (CH_2Cl_2, nm): 678, 648, 610, 355.
^{1}H NMR (300 MHz, CD_2Cl_2, δ, ppm): 9.91-9.88 (m, 4H); 9.66-9.64 (m, 4H); 8.10-8.05 (m, 4H); 1.52 (d, 9H); 1.50 (s, 9H); 1.48 (d, 9H); 1.46 (d, 9H); - 2.58 (t, 18H).
^{13}C NMR (151 MHz, CD_2Cl_2, δ, ppm): 154.4; 149.0; 134.3; 122.2; 119.6; 35.6; 31.3; -1.6.
HRMS: *m/z,* calcd. for $C_{54}H_{66}N_8O_2Si_3Na$: 965.45087; found: 965.45174.

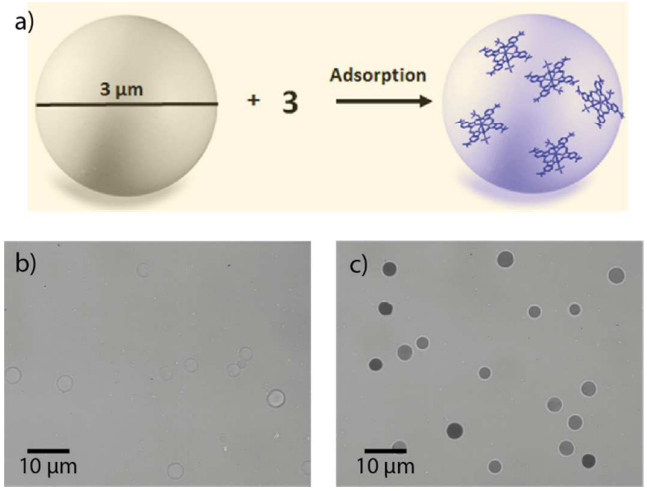

Figure 1. a) Schematic of the preparation of functionalized micro particles (**3@MP**). Bright field microscopy images of b) non-functionalized and c) functionalized silica microspheres.

Synthesis of 3@MP. 100 mg of spherical silica particles were suspended via sonication in 20 mL of toluene. 10 mg of **3** (0.01 mmol) was added to the suspension and sonication continued for 30 min. The toluene was removed by rotary evaporation, and the resulting blue material (**3@MP**) was suspended in 2 mL of deionized water and stored as aqueous suspension. The loading with **3** can therefore directly be derived from the amounts of educts, resulting in 10^{-7} mol / mg of **3@MP** particles.

Instrumentation used for photophysical analysis. Absorption spectra were measured on a Varian Cary 5000 double-beam UV-Vis-NIR spectrometer and baseline corrected. Steady-state emission spectra were recorded on a FluoTime300 spectrometer from PicoQuant equipped with a 300 W ozone-free Xe lamp (250-900nm), a 10 W Xe flash-lamp (250-900 nm, pulse width < 10µs) with repetition rates of 0.1 – 300 Hz, an excitation monochromator (Czerny-Turner 2.7 nm/mm dispersion, 1200 grooves/mm, blazed at 300 nm), diode lasers (pulse width < 80 ps) operated by a computer-controlled laser driver PDL-820 (repetition rate up to 80 MHz, burst mode for slow and weak decays), two emission monochromators (Czerny-Turner, selectable gratings blazed at 500 nm with 2.7 nm/mm dispersion and 1200 grooves/mm, or blazed at 1250 nm with 5.4 nm/mm dispersion and 600 grooves/mm), Glan-Thompson polarizers for excitation (Xe-lamps) and emission, a Peltier-thermostatized sample holder from Quantum Northwest (-40°C – 105°C), and two detectors, namely a PMA Hybrid 40 (transit time spread FWHM < 120 ps, 300 – 720 nm) and a R5509-42 NIR-photomultiplier tube (transit time spread FWHM 1.5 ns, 300-1400 nm) with external cooling (-80°C) from Hamamatsu. Steady-state and fluorescence lifetimes were recorded in TCSPC mode by a PicoHarp 300 (minimum base resolution 4 ps). Emission and excitation spectra were corrected for source intensity (lamp and grating) by standard correction curves. Lifetime analysis was performed using the commercial FluoFit software. The quality of the fit was assessed by minimizing the reduced chi squared function (χ^2) and visual inspection of the weighted residuals and their autocorrelation. Luminescence quantum yields were measured with a Hamamatsu Photonics absolute PL quantum yield measurement system (C9920-02) equipped with a L9799-01 CW Xenon light source (150 W), monochromator, C7473 photonic multi-channel analyzer, integrating sphere and employing U6039-05 PLQY measurement software (Hamamatsu Photonics, Ltd., Shizuoka, Japan). All solvents used were of spectrometric grade.

Singlet oxygen quantification. The relative singlet oxygen quantum yield (Φ_Δ) of **3** was determined by comparison with tetra-*t*-butylphthalocyaninato zinc(II) (**ZnPc**) as reference, and measured in CD_2Cl_2 in order to enhance the $^1O_2 \rightarrow {}^3O_2$ phosphorescence signal (Φ_Δ = 0.62, Daniel A. Fernández *et al.*, *Photochem. Photobiol.* **1996**, *63*, 784-792). The near infra-red phosphorescence spectrum of the photogenerated singlet oxygen was acquired and employed for the quantification of Φ_Δ. For this purpose, the area under the $^1O_2$ phosphorescence spectrum was plotted as a function of the fraction of absorbed light ($1\text{-}10^{-A}$) at three different concentrations for the reference and of the sample. The slopes of these plots (r_R and r_S respectively) are proportional to the corresponding Φ_Δ^R and Φ_Δ^S (where *R* stands for reference and *S* stands for sample). Thus, the Φ_Δ^S can be **estimated** according to Equation 1:

$$\Phi_\Delta^S = \Phi_\Delta^R \cdot \frac{r_S}{r_R} \qquad \text{Equation 1}$$

Singlet oxygen quantification in water. $^1O_2$ photogeneration rates of **3@MP** were derived using 9,10-anthracenediyl-*bis*(methylene)dimalonic acid (**ABMDMA**) as a fluorescent monitor (λ_{ex} = 380 nm) for photosensitized bleaching rates. Polychromatic irradiation from a projector lamp (Leica ZETT Royal II afs) passing through a cut-off filter at 610 nm was used to carry out the experiments. The Φ_Δ for the samples was calculated using Equation 2, where *r* is the slope of the **ABMDMA** bleaching over time (plotted as $\ln(F/F_0)$), $\lambda_1 - \lambda_2$ is the irradiation wavelength interval, $I_0(\lambda)$ the incident spectral photon flow, $A(\lambda)$ the absorbance, and the subscripts *R* and *S* are the reference (methylene blue, **MB,** Φ_Δ = 0.52, Francis Wilkinson et al., *J. Phys. Chem. Ref. Data*, **1993**, *22*, 113) and sample, respectively.

$$\Phi_\Delta^S = \Phi_\Delta^R \cdot \frac{r_S}{r_R} \cdot \frac{\int_{\lambda 1}^{\lambda 2} I_0(\lambda) \cdot (1-10^{-A_R(\lambda)}) \cdot d\lambda}{\int_{\lambda 1}^{\lambda 2} I_0(\lambda) \cdot (1-10^{-A_S(\lambda)}) \cdot d\lambda} \qquad \text{Equation 2}$$

The incident intensity can be approximated by a constant value, drawn out of the integral and cancelled.

Optical setup. For simultaneous optical manipulation and detection of bacterial damage by fluorescent dyes, HOT was combined with fluorescent microscopy in an inverted Nikon Eclipse Ti microscope. A schematic of the optical setup is depicted in Scheme 2. The light source used for optical trapping and organization of bacteria and particles was a Nd:YVO_4 laser (Smart Laser Systems, λ_{HOT} =1064 nm, P_{max} = 2.5W, TEM00 (M2 < 1.2)). This particular wavelength was selected in order to minimize the photodamage of the biological specimen as well as to avoid interaction with the

excitation wavelength of the functionalized particles. The laser power was adjusted to 50 mW (measured at the entrance of the inverted microscope) with a half-wave plate and a polarizing beam splitter (polarizing BS) in order to minimize the optical damage induced by the laser trapping beam but having at the same time enough power for simultaneous optical trapping of few bacteria. For the generation of multiple optical traps, a high resolution phase-only spatial light modulator (SLM) (Holoeye, Pluto, 1920x1080 pixels, full 2π phase range at λ = 1064 nm), was used together with a custom-made software and Camera 1 (PCO, Pixelfly qe) to modulate the laser beam and to tailor the desired trapping pattern in the front focal plane of a high numerical aperture microscope objective (MO, Nikon Apo TIRF, 100x/1.49 oil-immersion).

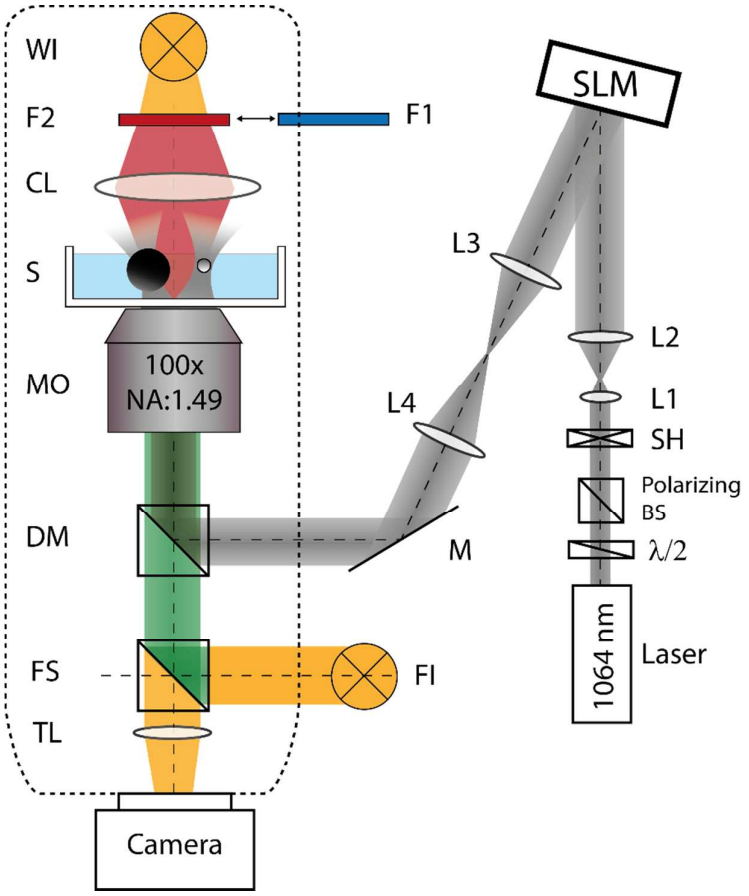

Scheme 2. Schematic representation of the optical setup used to perform the experiments. HOT elements: λ/2: half-wave plate, Polarizing BS: polarizing beam splitter, SH: shutter, L: lens, SLM: spatial light modulator, M: mirror, DM: dichroic mirror, MO: microscope objective, S: sample, WI: white light illumination, F: excitation filter, CL: condenser lens, FI: fluorescence illumination, FS; fluorescence filter set; TL: tube lens.

Bright field and fluorescence microscope images were obtained with the same microscope objective that was used for optical trapping. During optical arrangement of the bacteria near the particles, a band-pass excitation filter at 465-495 nm (F1)

was used in the bright field illumination system to avoid undesired single oxygen production by the microspheres. Once the bacteria were placed at specific distances from the particle's surface, the excitation filter was changed to 635-775 nm (F2) and the illumination intensity was set to the maximum irradiance available (320 mW), and fluorescence excitation was switched on to detect the incorporation of PI by the damaged bacteria. For PI detection, excitation with a mercury lamp for fluorescence microscopy was performed using a Cy3 filter set (Ex: 531/40, dichroic mirror: 562 nm, Em: 593/40). Images were recorded by a charge-coupled device (CCD) camera (ImagingSource) with an acquisition rate of two frames per minute and an exposure time of 0.363 sec.

Bacteria and culturing conditions. We used *Staphylococcus aureus* 6850 (J. M. Vann, et al. *Infect. Immun*. **1987**, *55*, 2155), as a model of bacterial microorganism. *S. aureus* is a Gram-positive, spherical bacterium with a diameter of about 1 μm. The slow motile behavior of *S. aureus* makes this type of bacteria an ideal candidate for our proof-of-principle study because the escape of the bacterium within an optical trap is avoided during long time measurements. Bacteria cells were cultivated overnight in Brain-heart infusion (BHI) medium at 36°C and later stored at -80°C. Prior the experiments, bacteria were defrosted, centrifuged at 5000 rpm for 2–3 minutes, and re-suspended at room temperature into *Phosphate-buffered saline* (PBS). To avoid fast cell division, the experiments were performed at room temperature.

Sample preparation and optical arrangement of particles and bacteria. Experiments were performed in ibidi-8-well chambers with PBS. PI was added to the PBS medium (1mg/ml) and used as a marker to determine loss of cell integrity. PI enters only in bacterial cell that have been damaged and have leaky membranes, forming a fluorescent complex with DNA, but it is not incorporated by bacteria that have an intact cell membrane. Functionalized microparticles and bacteria were separately pipetted into the sample, optically trapped with HOT and arranged at wish on the bottom of the wells' surface, depending on the HOT approach used for arrangement (for details, see the Results section). Before placing the bacteria near the particles, cell integrity was confirmed by the lack of PI fluorescence. In order to prevent optical trapping of unwanted specimens, the concentration of bacteria and particles was adjusted so that only few bacteria were visible within the field of view.

Data analysis. The time-trace of the PI signal allows identifying the moment when the ROS-induced cell damage is triggered by the optically excited functional microspheres. The fluorescence emission intensity of the PI was estimated from the average intensity in a small ROI of 27x27 pixels above each optically trapped bacterium. Once the cell membranes are irreversibly damaged, the fluorescence signal of PI is expected to rise quickly until photobleaching sets in. The increase of PI intensity was fitted with a linear function where the intersection of the slope with the background signal was defined as the point of activation for the onset of irreversible cell damage. Cells that showed no significant rise in the PI were considered alive during the whole experiment. Moreover, the loss of membrane potential should be irreversible and thus it could be considered that such cells die.

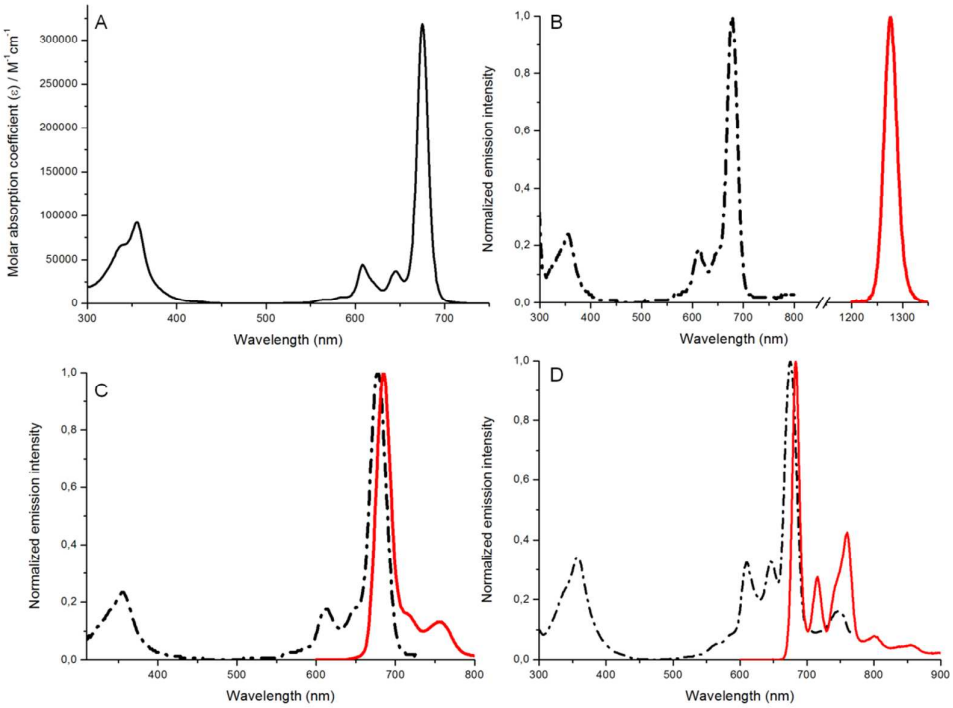

Figure 2. A) Molar absorption coefficient (ε) as function of wavelength for **3** in CH_2Cl_2. B) Fluorescence excitation and emission spectra (CH_2Cl_2, 10^{-5} M; λ_{exc} = 350 nm; λ_{em} = 758 nm). C) $^1O_2$ excitation and emission spectra (CD_2Cl_2, 10^{-5} M; λ_{exc} = 678 nm; λ_{em} = 1272 nm). D) Fluorescence excitation and emission spectra at 77 K in a glassy matrix of 2-methyltetrahydrofuran (10^{-5} M; λ_{exc} = 350 nm; λ_{em} = 800 nm).

Results and Discussion

Photophysical characterization

Steady-state and time resolved spectroscopy was performed on **3** in CH_2Cl_2 in order to be able to correlate the intrinsic photophysical characteristics of **3** with the properties of **3@MP** in water. In Figure 2, the spectra of **3** are depicted and show the

phthalocyaninates' typical Soret- and Q-absorption bands, the fluorescence as well as the $^1O_2$ phosphorescence profiles, which unambiguously prove the singlet oxygen photogeneration. Compound **3** has a fluorescence quantum yield of Φ_F = 0.61 and a singlet oxygen quantum yield of Φ_Δ = 0.44 as can be derived from Table 1. The capability to directly record the $^1O_2 \rightarrow {}^3O_2$ phosphorescence makes it possible to straightforwardly determine the $^1O_2$ quantum yield of **3** by comparison with **ZnPc** as a reference (Figure 3).

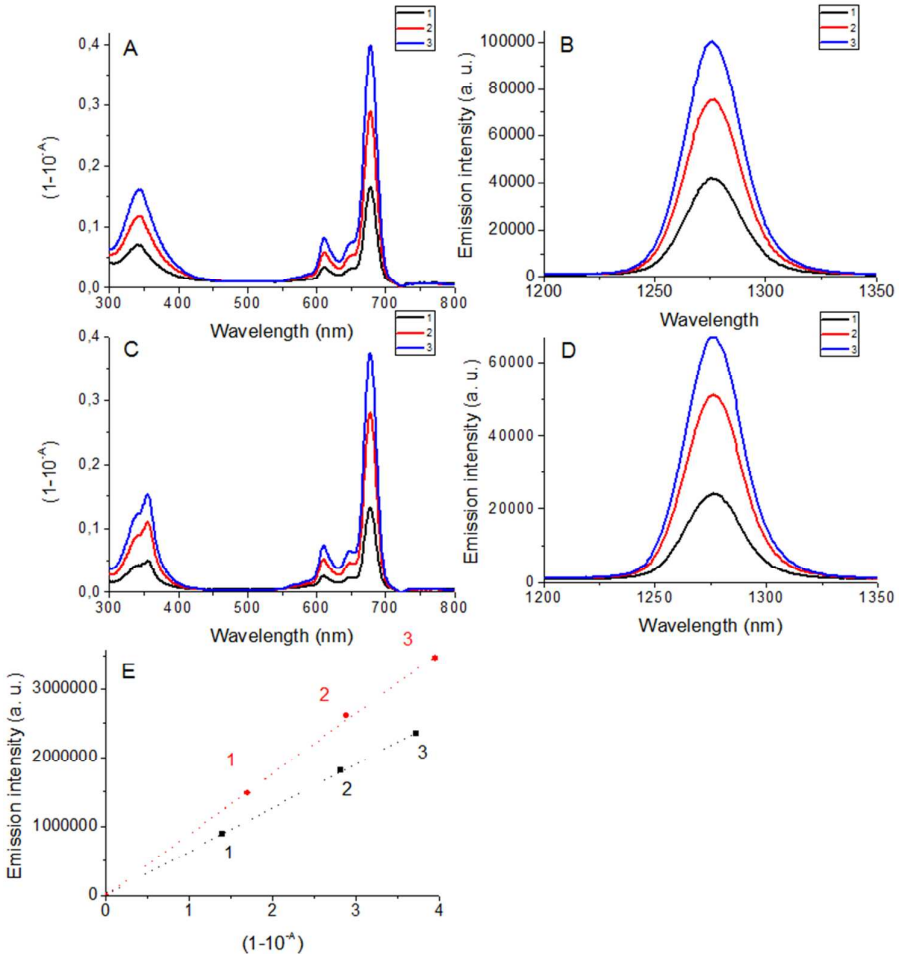

Figure 3. Absorption spectra of **ZnPc** (A) and **3** (C) and phosphorescence spectra of $^1O_2$ for **ZnPc** (B) and for **3** (D) at three different concentrations (sample 1: $3x10^{-7}$ M, sample 2: $5x10^{-7}$ M, and sample 3: $8x10^{-7}$ M). E) Plot of the emission intensity against the fraction of light absorbed for **ZnPc** (red dots) and for **3** (black dots) at three concentrations (sample 1: $2x10^{-7}$ M, sample 2: $4x10^{-7}$ M, and sample 3: $6x10^{-7}$ M).

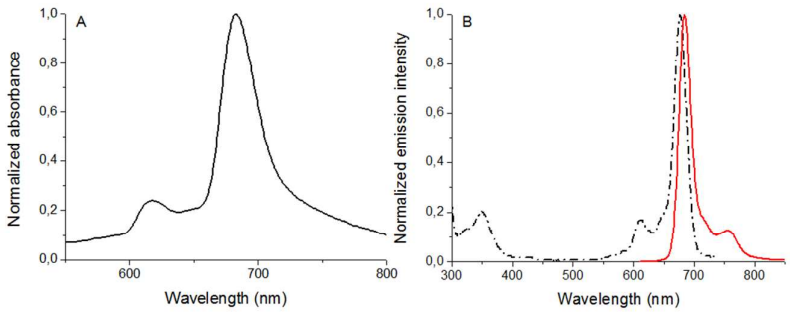

Figure 4. Baseline-corrected absorption spectrum of **3@MP** dispersed in water (A) and the corresponding fluorescence excitation and emission spectra (B; λ_{exc} = 350 nm; λ_{em} = 758 nm).

The hydrophobicity of **3** causes the formation of insoluble, photo-inactive aggregates in aqueous media. However, immobilization of **3** on the microparticles prevents this aggregation to a great extent and the photophysical features are retained in water, without possibility of uncontrolled passage into the aqueous phase, as no traces of 3 could be spectroscopically detected in the aqueous supernatants upon centrifugation. The characteristic near-infrared Q-band in the absorption spectrum and the fluorescence excitation and emission of aqueous suspensions of **3@MP** can be seen in Figure 4. Due to the weak phosphorescence of the $^1O_2 \rightarrow {}^3O_2$ transition even in deuterated water, the singlet oxygen quantum yield had to be determined indirectly by monitoring the fluorescence decay of a $^1O_2$ sensitive dye (**ABMDMA**). By comparing the rate of decay with **MB** as reference, Φ_Δ was calculated as described in the experimental section (Figure 5).

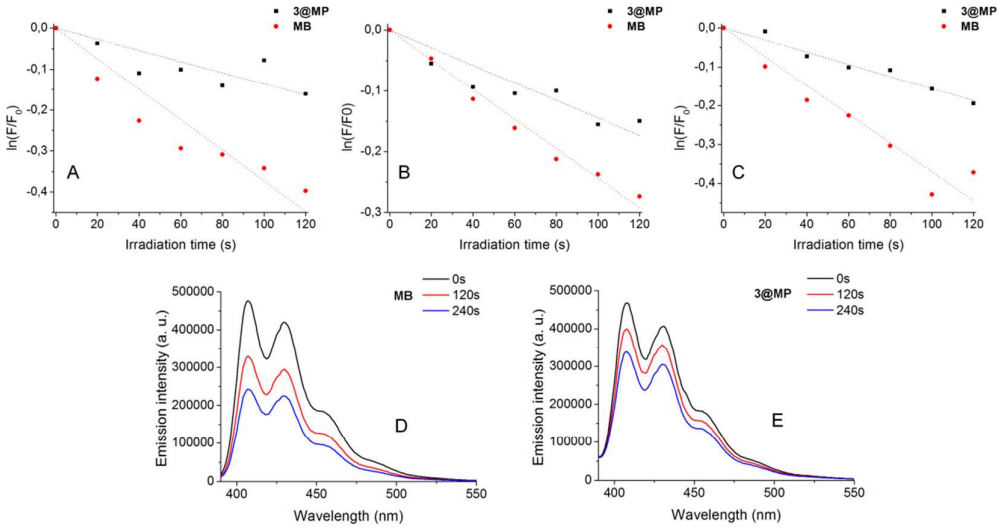

Figure 5. ABMDMA decay represented as $\ln(F/F_0)$ over time (measured as triplicates, experiments A, B, C) caused by the photoproduction of $^1O_2$ for **3@MP** and for **MB**. Emission spectra of **ABMDMA** monitored over time in the presence of **MB** (D) as a reference and of **3@MP** (E) (λ_{exc} = 380 nm).

Table 1. Photophysical properties of **3** in CH_2Cl_2 and of **3@MP** in H_2O.

Sample	Φ_F ± 0.02	Φ_Δ ± 0.05	λ_{abs} / nm (ε / $M^{-1}cm^{-1}$)	λ_{em} / nm at r. t. (at 77K)	τ / ns at r. t. (at 77K)
3	0.61 in CH_2Cl_2	0.44 in CD_2Cl_2	356, 610, 675 (92124, 42515, 318466)	684 (683)	5.07 (6.51)
3@MP	0.04 in H_2O	0.23 in H_2O	353, 615, 682 (-)	684 (-)	1.38, 4.00 (-)

With a singlet oxygen quantum yield of Φ_Δ = 0.23 we deduce that at least ½ of the chromophores are still available as active monomers for the generation of $^1O_2$ after the adsorption onto the microparticles in aqueous media, if referred to dilute solutions of **3** in CD_2Cl_2. Considering the hydrophobicity of **3** and the straightforward synthetic approach of adsorption, this is a notable performance that can be attributed to the bulky substituents at the tailored PS, which at least partially suppress the formation of inactive aggregates and energy traps, despite the fact that the adsorption process favors stacking.[31] A summary of all measured photophysical data of **3** as well as of **3@MP** can be found in Table 1. In principle, the ratio of the fluorescence quantum yield and the singlet oxygen quantum yield should be the same as for **3** in CD_2Cl_2 (namely Φ_F : Φ_Δ = 3 : 2) as both processes (fluorescence and intersystem crossing to the T_1 state which is responsible for the $^1O_2$ formation) start out from the same electronic excited S_1 state. However, this cannot be observed for **3@MP** in water, where the ratio is Φ_F : Φ_Δ = 1 : 6. The reason for this is most likely homo-FRET and inactive aggregates of **3** on the particles' surface. The excitons are funneled along the microparticle towards these dark energy traps and ultimately release their energy as heat, even though a residual ROS production seems to be possible. A similar behavior has been observed also for other Si(IV) phthalocyanines both at layered nanoclays[17] and in aqueous solution,[32] and can be attributed partially to the fact that J-aggregates have a lower but measurable Φ_F as compared to the monomeric species, while retaining a somewhat higher Φ_Δ. The shortened fluorescence lifetime for **3@MP** comparted to **3** also supports these hypotheses (5.07 ns (**3**) and 4.00 ns (**3@MP**)). The **3@MP** particles meet all the requirements that are needed for the $^1O_2$ inactivation for bacteria, making them suitable candidates for the proposed HOT studies.

Optical arrangement with microspheres deposited onto substrates and

bacteria held in suspension. The induced death of *S. aureus* 6850 bacteria in suspension was initially analyzed by approaching the bacteria towards surface-deposited **3@MP** microspheres with the aid of HOT.

The particles and bacteria have a high tendency to stick to the wells' surface in PBS medium. These adhesion forces are weak but still stronger than the ones typically exerted by the optical tweezers and strong enough to avoid detachment in the liquid medium. This adhesiveness was exploited for the initial experimental setup by depositing a **3@MP** suspension and optically trapping the particles while gliding down in the medium, and arranging them in specific and controlled configurations at the bottom of the wells. A suspension of *S. aureus* 6850 was then added to the sample chamber, and multiple bacteria were optically trapped and placed at variable distances *d* from the **3@MP** particles that were already stuck on the surface. The number of optically manipulated bacteria in each experiment typically ranged from 3-13 bacteria. During the placement of the bacteria, a band-pass excitation filter at 465-495 nm was used for the bright field illumination to avoid absorption of light by the PS and photoproduction of $^1O_2$ by **3@MP** (Figure 6b). Once the bacteria were placed at specific distances from the particle's surface, the filter in the bright field illumination was changed to a band-pass filter at 665-735 nm (Figure 6c) while the illumination intensity was set to the maximum irradiance available (320 mW). As it can be nicely seen in the absorbance spectrum of **3@MP** in aqueous suspension (Figure 4), **3@MP** is efficiently excited in this spectral region to produce $^1O_2$. In addition, excitation of the PI dissolved in the medium is avoided, as well as the associated heating of the sample.

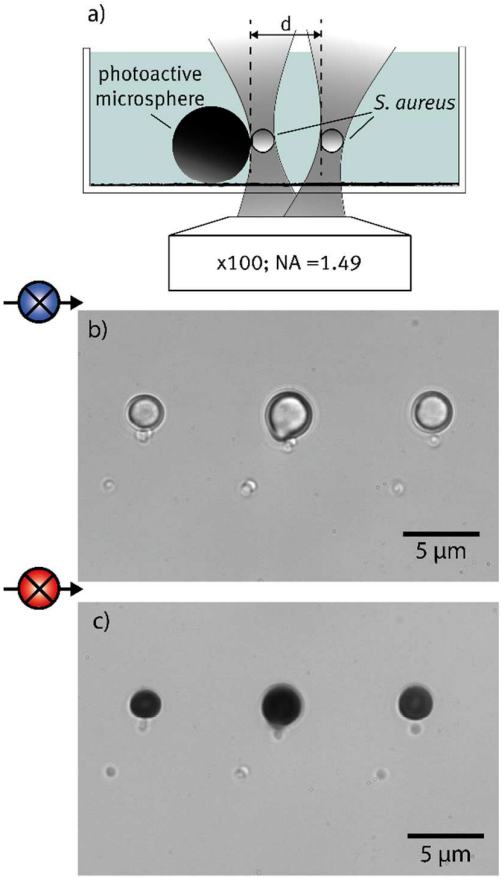

Figure 6: Optical placement of bacteria and PS-functionalized particles. (a) Schematic of the HOT-assisted manipulation and control of multiple bacteria at specific distances to the PC-functionalized microspheres which are previously attached on the glass substrate. (b)-(c) Bright-field images of an arrangement of bacteria and **3@MP** observed with an excitation filter in the illumination path at (b) 465-495 nm and (c) 665-735 nm.

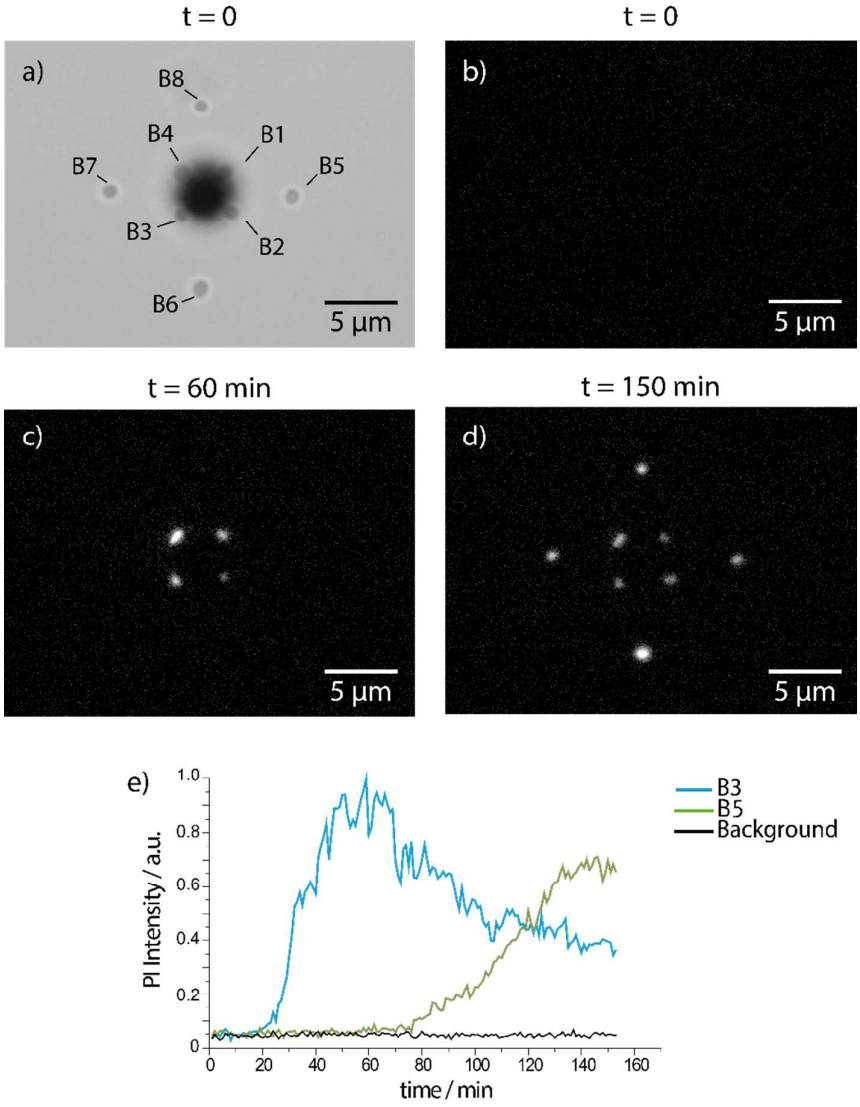

Figure 7: Monitoring cell damage by detection of PI incorporation with fluorescence microscopy. (a) Bright field microscopy image upon irradiation at 665-735 nm of four bacteria optically placed at the particle's surface (B1-B4) and at a separation distance of 3 µm (B5-B8). (b)-(d) Time-lapse of the microscopy images obtained by monitoring the PI-fluorescence of the bacterial configuration showed in (a) during the photoproduction of ROS. (e) Time-dependent fluorescence intensity plots of the incorporated PI.

Photoinduced inactivation of bacteria at different distances from the microspheres. In order to monitor the phototoxic effect of the irradiated **3@MP** particles on the bacteria, incorporation of PI by the cells was examined every 60 seconds using the corresponding fluorescence filter cube. Figure 7a shows the bright field illumination image of an exemplary configuration of eight bacteria, four of which were in direct contact with the microsphere (B1-B4) and the other four were placed at 3 µm away from the particle's surface (B5-B8). Figures 7b-d show the corresponding fluorescence microscopy images of the optically trapped bacteria upon continuous wide-field red light irradiation at 665-735 nm. The progressing inactivation is

observed by the increased emission of the PI signal due to the intercalation of PI into the bacterial DNA when the membrane is damaged. Figure 7e exemplary depicts the intensity curves of bacteria B3 and B5 as well as the background signal. After a defined time, a linear increase of the PI signal sets in and can be observed for all tested bacteria. This inflexion point is considered as the time at which the membrane integrity of the bacteria is irreversibly damaged, and therefore it is chosen as the diagnosis for bacterial death. In addition, it becomes clear that the fluorescence rise of the bacteria that are in closer proximity to **3@MP** show an intensity maximum which can be related to the point at which photobleaching of PI exceeds its uptake. The fluctuations in the fluorescence signal might be explained by the slight shift of the focus plane during the measurement.

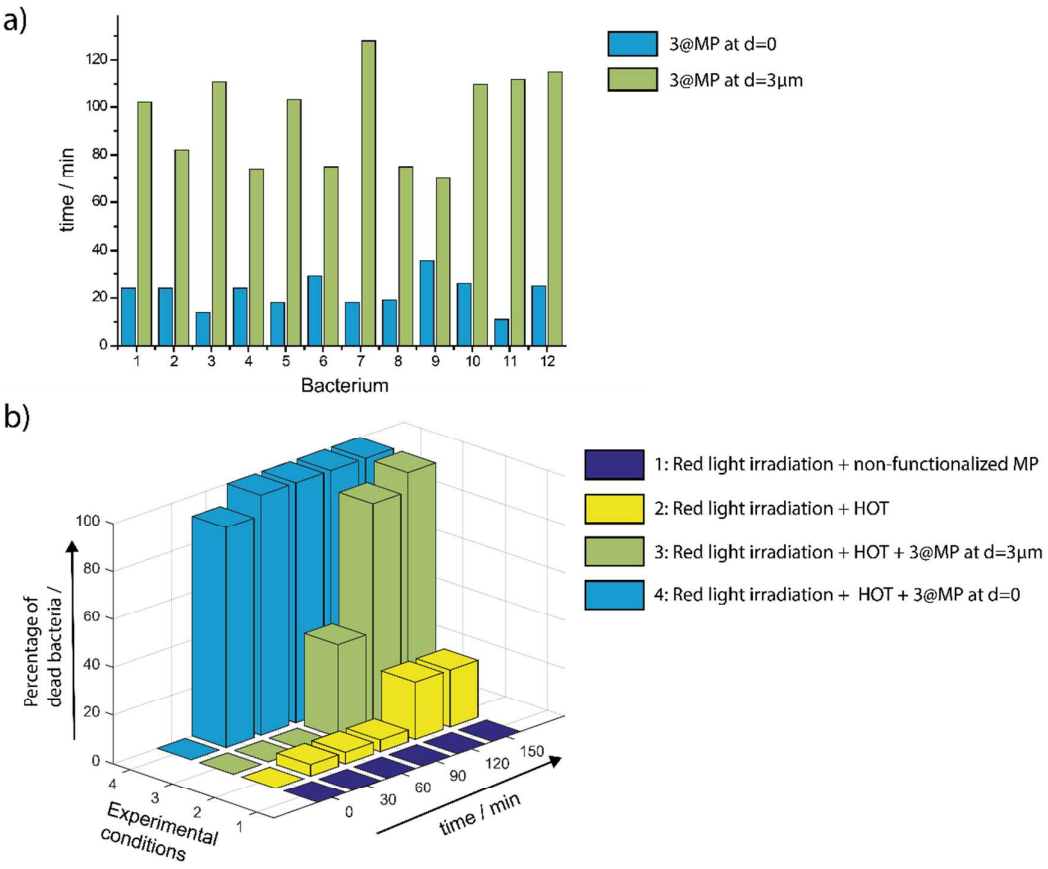

Figure 8: Analysis of photodynamic inactivation. (a) Irradiation time with red light required to damage the membrane of 12 bacteria attached to the **3@MP** and of 12 bacteria at a distance of 3 µm to the particle's surface. (b) Percentage of inactivated *S. aureus* as a function of time at different experimental conditions.

The irradiation time required for bacterial inactivation in the proximity of **3@MP** was systematically characterized by measuring the time at which bacteria start the incorporation of PI. Figure 8a shows the inactivation time of 12 optically arranged

bacteria close to the particles' surface (d = 0) in comparison with 12 bacteria placed at a distance of d = 3 µm. The required irradiation time for PI incorporation varies within a range of 12 to 35 min when individual bacteria cells are compared. However, in all cases, cell membrane degradation was measured 36 - 110 min earlier for those bacteria directly in contact to the **3@MP** particles. Quantification of the dead bacteria as a function of irradiation time is shown in Figure 8b. Also, it can be seen that only the concomitance of irradiation and photoactive **3@MP** particles led to the successful photoinactivation, thus confirming the photodynamic effect. No significant bacterial cell death was detected by the constant irradiation arising from the optical tweezers alone. A complete photodynamic inactivation was observed 36 min after irradiation for the cells that were in direct contact with the particle's surface, and after 130 min for the ones that were in a distance of 3 µm from the **3@MP** particles. This demonstrates the importance of proximity when it comes to the photoinduced inactivation of bacteria, but also that the cytotoxic effect reaches beyond the typical diffusion range of $^1O_2$ (268 nm).[33]

Optically-assisted arrangement of substrate-deposited bacteria and subsequent particle placement. With the aim of deeper analyzing the role of the bacterium-particle distance on the photoinduced inactivation, HOT's full 3D manipulation ability with controlled deposition on surfaces was used for the arrangement of bacteria and **3@MP** in an alternative way to the above-presented method. In this second approach, the inactivation of *S. aureus* 6850 bacteria was performed by first structuring a defined bacterial array and then approaching **3@MP** to them. For this purpose, a suspension of *S. aureus* 6850 was firstly provided, so that multiple bacteria were optically trapped and deposited in specific configurations onto the well's surface (Figures 9a, 9c). The typical number of optically manipulated bacteria in each experiment ranged from 10-50 bacteria. In this step, no particular illumination filter was taken into consideration, since there were no photoresponsive particles in the medium yet. A **3@MP** suspension was then added to the sample chamber and one particle at a time was deposited at a particular position on top of the bacterial array. During the placement of the particle, the band-pass excitation filter at 465-495 nm was used for the bright field illumination to avoid absorption of light by **3@MP** and photoproduction of $^1O_2$ (Figures 9b, 9d).

In comparison to the first HOT approach, this method presents a similar precision for the spatial manipulation of the bacteria and the functionalized microspheres. However, since a much lower irradiation with the optical trapping laser beam is required for arranging the desired bacterial configuration, a reduction of photo-

damage to the biological sample can be expected, which might be of crucial importance for other type of bacteria, and especially at other trapping wavelengths. In addition, the absence of optical traps during the photosensitization experiment allows avoiding the undesired particles or bacteria attraction into the field of view.

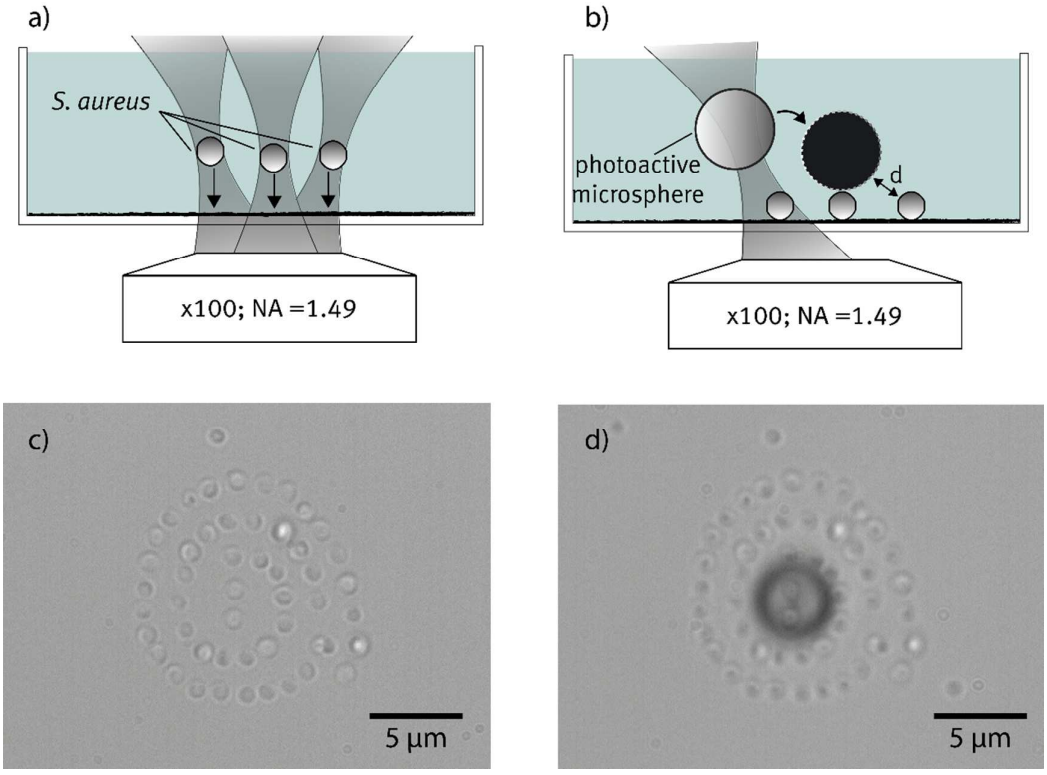

Figure 9: HOT-assisted organization of bacterial arrays and PS-functionalized particles. (a)-(b) Schematic of the HOT-assisted arrangement of multiple bacteria at specific distances on the microscopy substrate and the subsequent placement of a PC-functionalized microsphere onto the bacterial array. Bright field images of a bacterial array without (c) and with (d) the photoactive microsphere placed on top.

Quantitative spatio-temporal investigation of photoinduced bacterial inactivation. In order to analyze the dependence of the inactivation time with respect to the distance between the bacteria and the spot of $^1O_2$ production, the photodynamic treatment was applied to bacterial arrays that were arranged by the second HOT approach. Figure 10a shows the bright field illumination image of an exemplary array of 20 bacteria which were organized in a cross-like structure with 5 in-line bacteria in each of the four quadrants. The microsphere was placed at the crossing point to guarantee a direct contact with the four centered bacteria (B1-B4). The other bacteria are placed at specific separation distances between each other of 1 µm.

The viability of the bacterial cells was monitored by imaging the emission signal of the PI incorporated upon membrane damage. Figures 10b-d show the corresponding fluorescence microscopy images of the bacterial array after 0, 60, and 150 minutes of continuous wide-field irradiation at 665-735 nm. It can be observed that those bacteria in close contact with the microsphere were clearly inactivated after one hour of light exposure, while the surrounding bacteria required longer times for inactivation. After 150 minutes of photodynamic treatment, inactivation was achieved for 18 out of 20 bacteria, whereas 2 of the outer surviving cells showed no PI incorporation. It is to be noted that the rate of PI-uptake as well as the maximal PI emission of inactivated bacteria differs for each specimen so that the bacterial arrays typically show an inhomogeneous distribution of the PI emission.

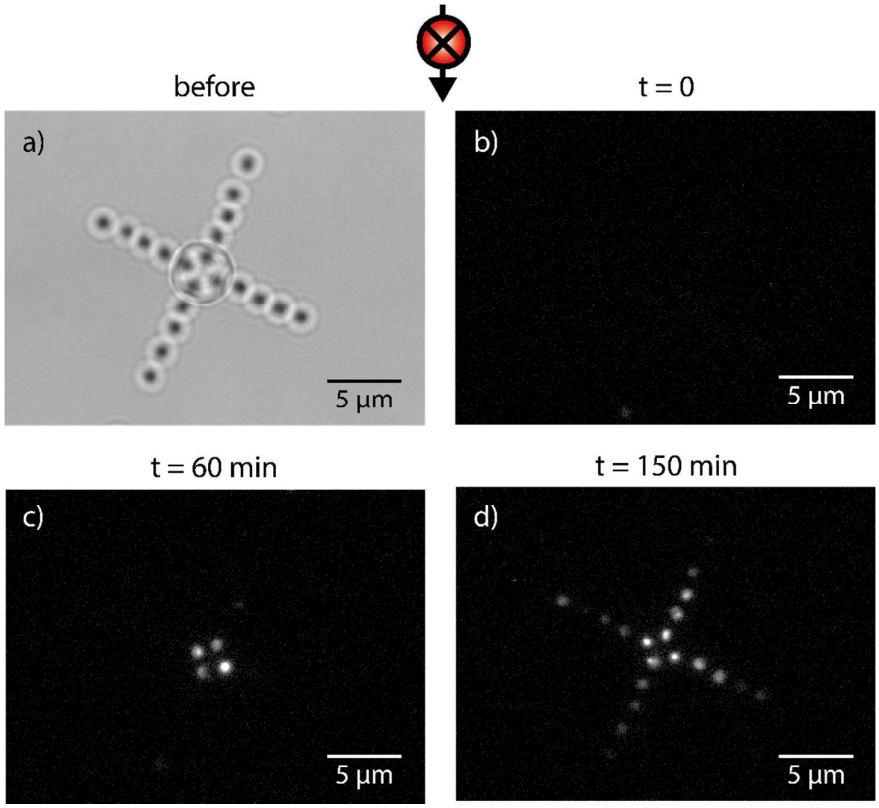

Figure 10: Monitoring the response to ROS of bacterial arrays with PS-functionalized particles in the center. (a) Bright field microscopy image of a structured array of 20 bacteria with a microsphere at the center. (b)-(d) Time-lapse fluorescence microscopy images of the bacterial configuration during the photodynamic treatment irradiating at 665-735 nm. The fluorescence arises from the incorporation of PI across the damaged membrane.

To quantitatively analyze the inactivation time of the bacteria with respect to the distance from the particle's interface, the same procedure was repeated with different bacterial arrays and photoactive **3@MP**. Figure 11a plots the inactivation time for a total amount of 70 bacteria, the data were obtained in 5 independent measurements

on 14 bacteria under similar experimental conditions each time. As it was shown in the first HOT approach, a clear spatial dependence is found for the irradiation time that was required to inactivate the bacteria. PI incorporation was produced between 6 and 40 min for the cells in close contact with the microsphere. Interestingly, no particular tendency is observed for the inactivation time of bacteria placed beyond 2 μm of the particle, which ranged from 80 to 180 minutes for longer distances. The significant difference (p<0.0001) between bacteria located in direct contact to the microparticle and at longer distances (Figure 11b) might be caused by different mechanisms of bacterial inactivation.[33] $^1O_2$ has a typical diffusion range of 268 nm,[9] and thus it might be responsible for damage of bacteria close to the microsphere. For bacteria located at further distances, inactivation might be explained by derived secondary ROS as e.g. superoxide and H_2O_2.[34]

The variance of the inactivation time of bacteria that are placed at similar distances to the particle could be explained by the diverse viability and resistance of each individual cell. In addition, inactivation times may vary between experiments because of the slightly different functionalization density of different particles (see Figure 1c). Despite these variations, the inactivation times that are measured by this second approach are in agreement with those presented in the first HOT approach.

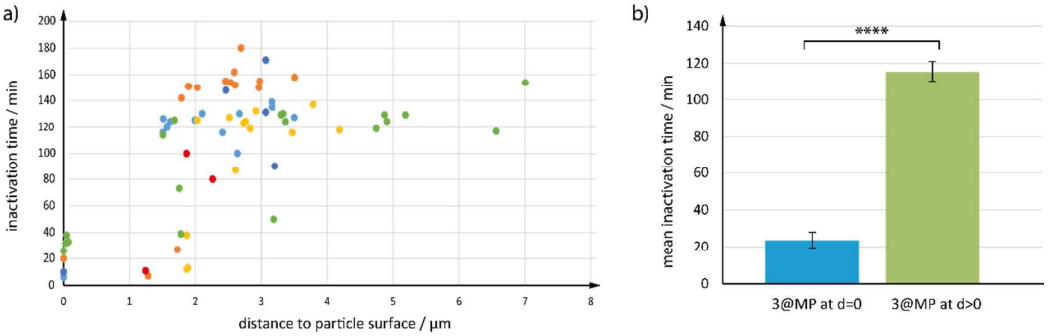

Figure 11: Distance dependence for the bacterial inactivation time. (a) Inactivation times measured for a total of 70 bacteria in different bacterial arrays as a function of the distance to the spot of $^1O_2$ production. The colors of the points correspond to the data obtained in five independent experiments. (b) Statistical analysis of the difference between the mean irradiation times required to inactivate bacteria that were located direct in contact with the **3@MP** and at longer distances. The asterisks represents an extremely statistically significant difference (p-value < 0.0001).

Conclusion

The development of quantitative spatiotemporally resolved methods is of utmost importance for a better understanding of the response of living systems to ROS. In this proof-of-principle study, we have presented a novel strategy based on the combination of holographic optical trapping and fluorescence microscopy for

quantifying at the single cell level the photoinduced cytotoxicity in a bacterial model. In comparison with established schemes and, owing to the sub micrometer precision of HOT, our method has the particular ability to control the position of bacteria with respect to the light-responsive microsphere representing a phototriggered source of ROS. This can be achieved with a high degree of accuracy, as it enables the controlled and switchable ROS production while monitoring the subsequent damage induced to bacterial cells. We have presented two versatile HOT approaches that allow arrangement of several bacteria around the PC-functionalized microsphere. These approaches permit investigating the minimal irradiation time that is required for bacterial inactivation as a function of the distance between the cells and the source of $^1O_2$ production.

Our results suggest that bacteria in close contact to the microspheres are probably inactivated by to the generation of $^1O_2$, whereas the death of distant bacteria might be explained by the longer diffusion ability of derived secondary ROS. Eventually this could be further investigated with the aid of specific fluorescent sensors that allow the direct imaging of different reactive oxygen species.[35,36] In addition, we demonstrated that only the concomitance of irradiation and the presence of photoactive **3@MP** particles influence the cell viability, proving the photodynamic treatment and confirming that our method is minimally invasive. Indeed, neither the trapping laser beam nor irradiation without microspheres induces serious damage to the investigated bacteria.

In summary, our method paves the way to bridge the gap between established approaches that measure the responses to ROS in the macroscopic and in the microscopic scales of bacterial ensembles and single cells, respectively. We are persuaded that the technique has a high potential to become a new tool in PDT and PDI for measuring the cytotoxic effect of other new PSs and on a variety of different living systems, and Gram-negative including Gram-positive bacteria, fungi, cancer cells and even swimming micro-organisms. Finally, our concept can be applied for the study of the inactivation of biological targets by other strategies, such as photothermal therapy.

Acknowledgment

This work was supported by the Deutsche Forschungsgemeinschaft in the frame of the German-Chinese TRR61. Further financial support by the DAAD RISE program is gratefully acknowledged.

References

(1) WHO. WHO | The Evolving Threat of Antimicrobial Resistance - Options for Action. *WHO Publ.* **2014**, 1–119.

(2) Fair, R. J.; Tor, Y. Antibiotics and Bacterial Resistance in the 21st Century. *Perspect. Medicin. Chem.* **2014**, *6*, 25–64.

(3) Dolmans, D. E. J. G. J.; Fukumura, D.; Jain, R. K. Photodynamic Therapy for Cancer. *Nat. Rev. Cancer* **2003**, *3* (5), 380–387.

(4) Huang, L.; Dai, T.; Hamblin, M. R. Antimicrobial Photodynamic Inactivation and Photodynamic Therapy for Infections. *Methods Mol. Biol.* **2010**, 635, 155−173.

(5) Sperandio, F. F.; Huang, Y.-Y.; Hamblin, M. R. Antimicrobial Photodynamic Therapy to Kill Gram-negative Bacteria. *Recent Pat. Anti-Infect. Drug Discovery* **2013**, 8 (2), 108−120.

(6) Chen, B.; Pogue, B. W.; Hoopes, P. J.; Hasan, T. Vascular and Cellular Targeting for Photodynamic Therapy. *Crit. Rev. Eukaryot. Gene Expr.* **2006**, *16* (4), 279–305.

(7) Castano, A. P.; Demidova, T. N.; Hamblin, M. R. Mechanisms in Photodynamic Therapy: Part One - Photosensitizers, Photochemistry and Cellular Localization. *Photodiagnosis Photodyn. Ther.* **2004**, *1* (4), 279–293.

(8) Ogilby, P. R. Singlet Oxygen: There Is Indeed Something New under the Sun. *Chem. Soc. Rev.* **2010**, *39* (8), 3181–3209.

(9) Circu, M. L.; Aw, T. Y. Reactive Oxygen Species, Cellular Redox Systems, and Apoptosis. *Free Radic. Biol. Med.* **2010**, *48* (6), 749–762.

(10) Pimenta, F. M.; Jensen, R. L.; Holmegaard, L.; Esipova, T. V.; Westberg, M.; Breitenbach, T.; Ogilby, P. R. Singlet-Oxygen-Mediated Cell Death Using Spatially-Localized Two-Photon Excitation of an Extracellular Sensitizer. *J. Phys. Chem. B* **2012**, *116* (34), 10234–10246.

(11) Fabregat, V.; Burguete, M. I.; Galindo, F.; Luis, S. V. Singlet Oxygen Generation by Photoactive Polymeric Microparticles with Enhanced Aqueous Compatibility. *Environ. Sci. Pollut. Res. Int.* **2014**, *21* (20), 11884–11892.

(12) Magaraggia, M.; Jori, G.; Soncin, M.; Schofield, C. L.; Russell, D. a. Porphyrin-Silica Microparticle Conjugates as an Efficient Tool for the Photosensitised Disinfection of Water Contaminated by Bacterial Pathogens. *Photochem. Photobiol. Sci.* **2013**, *12* (12), 2170–2176.

(13) Acosta, M. A.; Velasquez, M.; Williams, K.; Ross, J. M.; Leach, J. B. Fluorescent Silica Particles for Monitoring Oxygen Levels in Three-Dimensional Heterogeneous Cellular Structures. *Biotechnol. Bioeng.* **2012**, *109* (10), 2663–2670.

(14) Baumes, J. M.; Gassensmith, J. J.; Giblin, J.; Lee, J.-J.; White, A. G.; Culligan, W. J.; Leevy, W. M.; Kuno, M.; Smith, B. D. Storable, Thermally Activated, near-Infrared Chemiluminescent Dyes and Dye-Stained Microparticles for Optical Imaging. *Nat. Chem.* **2010**, *2* (12), 1025–1030.

(15) Strassert, C. A.; Otter, M.; Albuquerque, R. Q.; Hone, A.; Vida, Y.; Maier, B.; De Cola, L. Photoactive Hybrid Nanomaterial for Targeting, Labeling, and Killing Antibiotic-Resistant Bacteria. *Angew. Chemie - Int. Ed.* **2009**, *48* (42), 7928–7931.

(16) Grüner, M.; Siozios, V.; Hagenhoff, B.; Breitenstein, D.; Strassert, C. A. Structural and Photosensitizing Features of Phthalocyanine - Zeolite Hybrid Nanomaterials. *Photochem. Photobiol.* **2013**, *89* (6), 1406–1412.

(17) Grüner, M.; Tuchscherr, L.; Löffler, B.; Gonnissen, D.; Riehemann, K.; Staniford, M. C.; Kynast, U.; Strassert, C. A. Selective Inactivation of Resistant Gram-Positive Pathogens with a Light-Driven Hybrid Nanomaterial. *ACS Appl. Mater. Interfaces* **2015**, *7* (37), 20965–20971.

(18) Staniford, M. C.; Lezhnina, M. M.; Gruener, M.; Stegemann, L.; Kuczius, R.; Bleicher, V.; Strassert, C. A.; Kynast, U. H. Photophysical Efficiency-Boost of Aqueous

Aluminium Phthalocyanine by Hybrid Formation with Nano-Clays. *Chem. Commun.* **2015**, *51* (70), 13534-13537.

(19) Mirenda, M.; Strassert, C. A.; Dicelio, L. E.; Román, E. S. Dye-Polyelectrolyte Layer-by-Layer Self-Assembled Materials: Molecular Aggregation, Structural Stability, and Singlet Oxygen Photogeneration. *ACS Appl. Mater. Interfaces* **2010**, *2* (6), 1556–1560.

(20) Voskuhl, J.; Kauscher, U.; Gruener, M.; Frisch, H.; Wibbeling, B.; Strassert, C. a.; Ravoo, B. J. A Soft Supramolecular Carrier with Enhanced Singlet Oxygen Photosensitizing Properties. *Soft Matter* **2013**, *9* (8), 2453–2457.

(21) Stegemann, L.; Schuermann, K. C.; Strassert, C. A.; Grecco, H. E. Photofunctional Surfaces for Quantitative Fluorescence Microscopy: Monitoring the Effects of Photogenerated Reactive Oxygen Species at Single Cell Level with Spatiotemporal Resolution. *ACS Appl. Mater. Interfaces* **2015**, *7* (10), 5944–5949.

(22) Neuman, K. C.; Block, S. M. Optical Trapping. *Rev. Sci. Inst.* **2004**, *75*, 2787–2809.

(23) Zhang, H.; Liu, K.-K. Optical Tweezers for Single Cells. *J. R. Soc. Interface* **2008**, *5* (24), 671–690.

(24) Haruff, H. M.; Munakata-Marr, J.; Marr, D. W. M. Directed Bacterial Surface Attachment via Optical Trapping. *Colloids Surfaces B Biointerfaces* **2003**, *27* (2), 189–195.

(25) Woerdemann, M.; Hörner, F.; Denz, C. Structured Attachment of Bacterial Molecular Motors for Defined Microflow Induction. *Optofluid. Microfluid. Nanofluid.* **2014**, *1* (1), 19–26.

(26) Simpson, K. H.; Bowden, M. G.; Höök, M.; Anvari, B. Measurement of Adhesive Forces between S. Epidermidis and Fibronectin-Coated Surfaces Using Optical Tweezers. *Lasers Surg. Med.* **2002**, *31* (1), 45–52.

(27) Jones J.F., V. D. Laser Trap Studies of End-on E. Coli Adhesion to Glass. *Colloids Surf., B* **2006**, *50* (1), 66–71.

(28) Grier, D. G. A revolution in optical manipulation. *Nature* **2003**, *424* (6950), 810–816.

(29) Barroso, Á.; Landwerth, S.; Woerdemann, M.; Alpmann, C.; Buscher, T.; Becker, M.; Studer, A.; Denz, C. Optical Assembly of Bio-Hybrid Micro-Robots. *Biomed. Microdevices* **2015**, *17* (2), 1–8.

(30) Hörner, F.; Woerdemann, M.; Müller, S.; Maier, B.; Denz, C. Full 3D Translational and Rotational Optical Control of Multiple Rod-Shaped Bacteria. *J. Biophoton.* **2010**, *3* (7), 468–475.

(31) Rodríguez, H. B.; San Román, E. Effect of Concentration on the Photophysics of Dyes in Light-Scattering Materials. *Photochem. Photobiol.* **2013**, *89* (6), 1273–1282.

(32) Galstyan, A.; Block, D.; Niemann, S.; Grüner, M. C.; Abbruzzetti, S.; Oneto, M.; Daniliuc, C. G.; Hermann, S.; Viappiani, C.; Schäfers, M.; Löffler, B.; Strassert, C. A.; Faust, A. Labelling and Selective Inactivation of Gram-positive bacteria Employing Bimodal Photoprobes With Dual Readouts. *Chem Eur. J.* **2016**, DOI:10.1002/chem.201504935.

(33) Skovsen, E.; Snyder, J. W.; Lambert, J. D. C.; Ogilby, P. R. Lifetime and Diffusion of Singlet Oxygen in a Cell. *J. Phys. Chem. B* **2005**, *109* (18), 8570–8573.

(34) Krumova, K.; Cosa, G. Chapter 1: Overview of Reactive Oxygen Species. **2016**.

(35) Oleynik, P.; Ishihara, Y.; Cosa, G. Design and Synthesis of a BODIPY-α-Tocopherol Adduct for Use as an Off/On Fluorescent Antioxidant Indicator. *J. Am. Chem. Soc.* **2007** *129* (7), 1842–1843.

(36) Pedersen, S. K.; Holmehave, J.; Blaikie, F. H.; Gollmer, A.; Breitenbach, T.; Jensen, H. H.; Ogilby, P. R. Aarhus sensor green: A fluorescent probe for singlet oxygen. *J. Org. Chem.* **2014**, *79* (7), 3079–3087.

Table of Contents Graphic